RAPID COMMUNICATIONS IN MASS SPECTROMETRY
Rapid Commun. Mass Spectrom. 2010; **24**: 1911–1918
Published online in Wiley InterScience (www.interscience.wiley.com) DOI: 10.1002/rcm.4592

RCM

Theoretical and experimental study of the achievable separation power in resistive-glass atmospheric pressure ion mobility spectrometry

Mark Kwasnik and Facundo M. Fernández*
School of Chemistry and Biochemistry, Georgia Institute of Technology, Atlanta, GA 30332, USA

Received 9 March 2010; Revised 19 April 2010; Accepted 20 April 2010

We present a detailed investigation of the performance of our previously reported nanoelectrospray high-resolution resistive-glass atmospheric pressure drift tube ion mobility spectrometer constructed with monolithic resistive-glass desolvation and drift regions. Using experimental spectral data and theoretical pulse width and diffusion variables, we compare theoretical and experimental resolving powers achievable under a variety of field strengths and ion gate pulse widths. The effects of instrumental and operational parameters on the resolution achievable in chromatographic terms are also discussed. Following characterization of the separation power of the instrument, experimental spectral peak width data is fitted by a least-squares procedure to a pre-existing semi-empirical model developed to study contributions to peak width other than initial pulse width and diffusional broadening. The model suggests possible contributions to the final measured peak width from electric field inhomogeneity and minor contributions from instrumental parameters such as anode size, anode-to-anode grid distance and drift gas flow rate. The model also reveals an unexpected ion gate width dependence on the final measured peak width that we attribute to non-ideal performance of the Bradbury-Nielsen ion gate and limitations in the design of our pulsing-electronics. Copyright © 2010 John Wiley & Sons, Ltd.

Drift tube ion mobility spectrometry (DTIMS) is a rapid post-ionization gas-phase separation technique that separates compounds based on their differences in reduced mass, charge, and collisional cross-section under a weak, time-invariant electric field. The DTIMS technology, first introduced as plasma chromatography in 1970,[1] can trace its origins to the ion mobility theory developed before 1910.[2] In the past decade, there has been a substantial increase in the development of new IMS technologies that can subsequently be coupled to mass spectrometry (MS). Coupling DTIMS to MS adds a semi-orthogonal separation dimension that can be used to distinguish isomeric compounds,[3] closely related ionic species,[4] and that provides valuable structural information that can be utilized for determination of gas-phase ion conformation.[5–8] DTIMS is routinely applied to a variety of problems including the analysis of chemical warfare agent degradation products,[9] explosives,[10] pharmaceuticals,[11] narcotics,[12–14] and environmental pollutants.[15] In addition, the use of IMS in multidimensional separations for comprehensive proteomic experiments has led to a better understanding of complex biological systems.[16–18]

As with any other separation technique, the ability of DTIMS to resolve closely spaced peaks is of paramount importance. To this end, Hill and co-workers have studied the effects of several experimental variables on the resolving power of atmospheric pressure IMS. Their results consistently showed that peaks in DTIMS spectra had a larger temporal width than predicted, even after accounting for differences in instrument design, initial pulse width and thermal ion diffusion. In order to rationalize these differences, they proposed that Coulombic repulsions and electric field inhomogeneities within the drift tube were responsible for the lower than ideal resolving powers observed.[19]

Currently, most ion mobility spectrometers utilize a drift region built with a stack of ring electrodes, each pair separated by insulating spacers. In contrast, our recently described DTIMS system is furnished with resistive-glass monolithic desolvation and drift chambers.[20] Resistive-glass is a lead silicate glass that has been reduced in a hydrogen atmosphere to make its surface semiconducting.[21] Kelvin probe measurements show that resistive-glass produces highly uniform electrical fields.[22] The use of resistive-glass for building ion mobility spectrometers has four advantages: (1) the radial inhomogeneities in the drift tube electric field are minimized compared with a conventional stacked ring drift tube; (2) the construction of ion mobility spectrometers is simplified, eliminating the need for machining several ring electrodes and using resistor chains to generate the potential gradient; (3) the complexity of periodic cleaning and maintenance is reduced; and (4) the resistive-glass is rugged making it suitable for field applications while maintaining mechanical integrity.

Here we present a detailed investigation of the performance of our previously reported high-resolution monolithic

**Correspondence to*: F. M. Fernández, School of Chemistry and Biochemistry, Georgia Institute of Technology, Atlanta, GA 30332, USA.
E-mail: facundo.fernandez@chemistry.gatech.edu

RCM

resistive-glass based DTIMS system[20] using experimental spectral data in comparison with theoretical pulse width and diffusion variables. We also incorporate the theory of Siems *et al.*[19] and utilize their semi-empirical models to provide a means of studying instrumental design factors and investigating the effect of such factors on instrumental performance. Contributions to measured peak widths from factors such as radial electrical field variations within the drift tube caused by the resistive-glass building material are explored. The model employed here also provides an indirect means to study the performance of the Bradbury-Nielsen ion gate (BNG) in our spectrometer. These types of ion gates are known to perform non-ideally and were shown to produce ion packets with a slowly decaying population at their leading and trailing edges.[23] SIMION modeling has also portrayed this phenomenon by modeling the distortion effects caused by wire grids on ions under atmospheric pressure conditions.[24,25]

The IMS resolving power (R_p) is defined as the ratio between the drift time (t_d) and the full peak width at half maximum (w) (i.e. $R_p = t_d/w$). The shape of an IMS peak is determined by the initial shape of the ion packet injected (t_g) into the drift tube by the BNG[26] and the diffusional broadening contribution (t_{diff}) for the ion packet as it travels through the drift space to the detector. (i.e. $w^2 = t_g^2 + t_{diff}^2$). The t_{diff}^2 parameter has been expanded by Revercomb and Mason to the following:[27]

$$t_{drift}^2 = \frac{16 \ln 2 k T t_d^2}{qV} \quad (1)$$

This expanded equation was later re-written by Siems *et al.* to include three adjustable parameters; α, β, and γ, that could be applied to experimental line width data to evaluate various contributions to experimentally measured peak widths, resulting in the following equation:

$$w^2 = \gamma + \beta t_g^2 + \alpha \frac{T t_d^2}{V} \quad (2)$$

where α represents the diffusion contribution to the final observed pulse width. Assuming ideal behavior, α would have a value of 0.957×10^{-3}. A larger value would indicate effects such as field inhomogeneity, energy imparted by the electric field or other such effects. The β term describes the contribution from ion gating to the final observed pulse width. Assuming ideal gating and no diffusion, the width of the injected ion packet would be the width of the final measured ion packet yielding an ideal value of $\beta = 1$. Changes in β would indicate non-ideal performance of the BNG or non-diffusional contributions to packet broadening such as Coulombic repulsion that would be dependent on the quantity of ions injected with each packet. The γ term is an instrument-specific constant that accounts for any parameters not affected by gating or voltage and it would have an ideal value of zero.

In the work presented here, this semi-empirical model is applied to evaluate not only contributions to pulse width from factors such as field inhomogeneity and gate performance in our resistive-glass IM spectrometer, but also contributions from other instrumental parameters such as anode size, anode-to-anode grid distance, drift gas flow rate, and their effects on resolving power. Also presented is an investigation of the effect of drift voltage, anode size, anode to anode grid distance, and drift gas flow rate on the analytical separation power of our instrument, measured as the chromatographic resolution:[28,29]

$$R = \frac{t_{d2} - t_{d1}}{(w_{b1} + w_{b2})/2} \quad (3)$$

where w_b is the peak width at the base of two consecutive peaks.

EXPERIMENTAL

Reagents and samples

The solvent used for all nanoelectrospray experiments was a mixture of acetonitrile (HPLC grade, Burdick & Jackson, Muskegon, MI, USA) and high-purity water (18.2 MΩ cm^{-1}, Barnstead Nanopure Diamond, Van Nuys, CA, USA) in a 70:30 volume ratio. Sample solutions of tetrabutylammonium (TBA) nitrate (98%, Acros, Geel, Belgium) and tetraethylammonium (TEA) acetate tetrahydrate (99%, Sigma-Aldrich, St. Louis, MO, USA) were prepared and analyzed at concentrations of 150 μM. Nitrogen (99.9997%, Airgas, Atlanta, GA, USA) was used as the drift gas.

Resistive-glass ion mobility spectrometer

As the IMS configuration and operating procedures have been described in detail in our previous publication,[20] only a brief description is presented here. A schematic diagram of the longitudinal cross-section of the resistive glass ion mobility spectrometer showing the nanoESI source, ion gate, anode grid, anode, and power supply connections is shown in Fig. 1. The desolvation and drift regions were constructed of monolithic sections of resistive-glass tubes (Photonis, Sturbridge, MA, USA) with a resistance of 0.45 GΩ cm^{-1}. The dimensions of the tubes were 3 cm i.d. and 4 cm o.d. with lengths of 12 cm and 26 cm for the desolvation and drift regions, respectively. A power supply (FUG HCL 14-2000, Magnavolt Technologies, Plattsburgh, NY, USA) was used to provided adequate high voltages through a voltage divider,

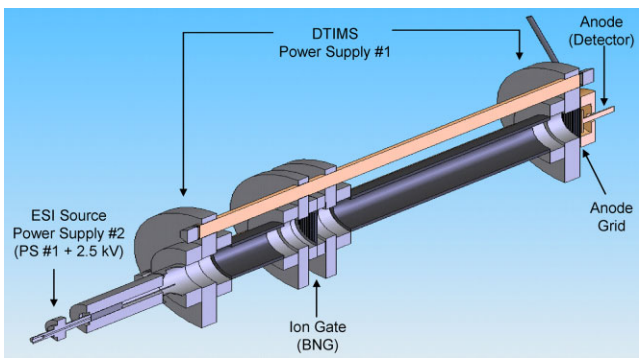

Figure 1. Schematic of the longitudinal cross-section of the resistive-glass ion mobility spectrometer showing the nanoESI source, ion gate, anode gride, and anode. Power supply #1 is used to apply voltage to the IMS system and power supply #2 is used to apply voltage for the nanoESI source (set +2.5 kV higher than power supply #1).

DOI: 10.1002/rcm

for the entrance and exit of the desolvation and drift tubes and for the grid electrode which was placed 5 mm in front of the Faraday plate detector (TOFWERK AG, Thun, Switzerland).

The nanoESI source was equipped with a 50 μm i.d. SilicaTip emitter (PicoTip, New Objective Inc., Woburn, MA, USA) and was operated at a flow rate of 200–400 nL min^{-1} without the assistance of sheath gas. The position of the nanoESI emitter was adjusted so that it penetrated 1.5 cm into the desolvation region. High voltage was applied to the sprayed solution via an electrochemical junction placed 30 cm upstream from the emitter tip. Sample solution was delivered to the ESI source by a liquid handling pump (VICI M6, Valco Instruments Co., Houston, TX, USA) connected to the tip using PEEK capillary tubing (100 μm i.d., 360 μm o.d., 1571, Upchurch, Oak Harbor, WA, USA). A second high-voltage power supply (FUG HCP 14-2000, Magnavolt Technologies) provided independent voltage control for the nanoESI source. An electrospray voltage of +2.5 kV vs. the desolvation chamber entrance was used for all experiments.

Drift gas at a flow rate of 0.2 L min^{-1}, unless otherwise noted, was supplied to the IMS instrument through a custom-built gas diffuser positioned behind the detector. This flow rate was controlled via a precision flow meter/controller (PMR1, BEL-ART/Scienceware, Pequannock, NJ, USA). Prior to entering the drift chamber, the drift gas was purified and dried by a moisture trap (Restek 22015, Bellefonte, PA, USA).

Ion beam gating was achieved with a Bradbury-Nielsen-type ion gate[26] located between the end of the desolvation tube and the entrance of the drift tube. Custom-built push-pull pulsing electronics powered this ion gate. The logic signals required to trigger the pulsing electronics were generated through a PC (AMD Athlon XP 2600+ 1.91 GHz, 1.0 GB RAM) equipped with an arbitrary waveform generator board (National Instruments 5411, Austin, TX, USA). The ion gate was closed by applying ±35 V to adjacent wire sets causing positive ions to be collected on the negative wire set and negative ions to be collected on the positive wire set. Ion gate pulse widths of 800, 400, 200 and 100 μs were investigated. The chosen ion gate triggering sequence length and modulation bin width, alternatively referred to as the ion gate pulse width, were downloaded to the arbitrary waveform generation board by the user via software coded in LabView 7.0 (National Instruments).

A Faraday plate detector mounted at the end of the drift tube 5 mm behind an anode grid was connected to a custom-built amplifier (TOFWERK AG). Data from this amplifier was acquired and saved in tab-delimited text format using a fast 12-bit 5 Msamples s^{-1} A/D data acquisition board (National Instruments 6111) synchronized with the 5411 arbitrary waveform generator via its 20-MHz clock. Data collected with a modulation bin width of 100 and 200 μs was oversampled by a factor of four, while data collected with modulation bin widths of 400 and 800 μs was oversampled by a factor of eight with respect to the modulation bin width, and 100 sweeps were averaged for all collected spectra.

Variable voltage studies

Voltage-dependent experiments were performed by operating both the nanoESI source and the IMS high-voltage power supplies in a synchronous manner. The IMS power supply was set to provide a 15 kV voltage to the entrance of the desolvation chamber while the electrospray power supply was operated with a voltage of +2.5 kV with respect to the instrument power supply (see Fig. 1). The two power supplies were then adjusted synchronously to produce a 1 kV stepwise change in voltage at the entrance of the desolvation chamber. The voltage was reduced in 1 kV increments until a signal could no longer be observed. The number of voltage reduction steps was dependent on the size of the ion gate, with larger ion gates allowing for collection of spectra at lower voltages. The voltage at the start of the drift chamber was calculated based on the starting voltage applied to the voltage divider. Measurements of drift time, peak width, and peak width at half-height were made over a range of drift voltages, ion gate pulse widths, and instrumental parameters for both the TBA and the TEA ions. Instrumental parameters such as anode size (10 and 30 mm), anode-to-anode grid (AG) distance (5.0 and 0.7 mm), drift gas flow rate (0.2 and 1.5 L min^{-1}) and their effects on resolving power and separation power in terms of chromatographic resolution were investigated.

The information was used to calculate the change in resolving power for the two analyte ions. The theoretical 'ideal' resolving power was calculated as a function of voltage and gate pulse width for comparison with the experimentally observed resolving powers, to determine conditions for the optimal resolving power. Voltage-dependent data was then plotted, and a least-squares fit was used to determine the most accurate α, β, and γ parameters.

Safety considerations

High voltages are used in this type of instrument and only personnel with proper training should operate it. Warning signs should be posted in the surroundings of the instrumental setup to ensure that no accidental exposure to high voltage occurs.

RESULTS AND DISCUSSION

Figure 2 shows both the theoretical and the experimental R_p for the TBA and TEA ions using 800, 400, 200 and 100 μs ion gate widths and drift voltages in the range 5.84–11.58 kV for the 10 mm anode, 5.0 mm AG distance instrumental configuration. The blue (diamonds) and green (squares) traces represent the theoretical R_p for TBA and TEA, respectively, while the red (triangles) and black (circles) traces represent experimentally obtained R_p values for TBA and TEA. It was observed that each ion gate width has an optimal operational drift voltage that maximizes R_p, with larger ion gate widths (top panels) performing better at lower drift voltages and shorter ion gate widths (bottom panels) performing slightly better at higher drift voltages. The experimental performance for all ion gate widths was lower than the theoretically achievable maximum value of R_p. These results are consistent with work performed by Watts and Wilders[30] who showed that for a selection of three different instruments, experimentally obtained R_p values for all ion gate widths were 'under-achieving' by approximately 50%.

DOI: 10.1002/rcm

RCM

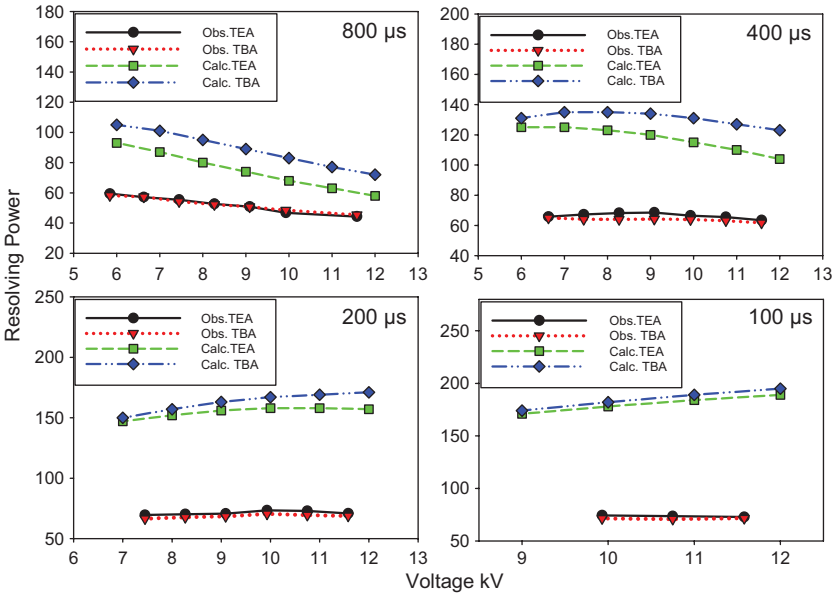

Figure 2. Theoretical and experimental resolving power (R_p) obtained for 150 µM tetrabutylammonium (TBA) nitrate and tetraethylammonium (TEA) acetate tetrahydrate solutions using 800, 400, 200 and 100 µs ion gate widths and drift voltages in the range 5.84–11.58 kV for a 10-mm-diameter anode and a 5.0 mm anode grid distance instrumental configuration. The blue (diamonds) and green (squares) traces represent the theoretical R_p for TBA and TEA, respectively, while the red (triangles) and black (circles) traces represent experimentally observed values. A drift gas at a flow rate of 0.2 L min^{-1} was used.

Detailed consideration of the data shown in Fig. 2 reveals that the difference between the theoretical and experimental values of R_p increased as the ion gating pulse width was made shorter. For example, the experimentally obtained R_p of TEA acquired at a 10 kV drift voltage and an 800 µs gate was 25% lower than the expected value. The difference between theoretical and experimental R_p increased to 45, 55, and 60% for ion gate widths of 400, 200, and 100 µs, respectively. This increase in under-performance at shorter gates indicated a possible constant error contribution from imperfect gating and will be addressed further in the following sections. The data also revealed that, although the theoretical R_p for TEA and TBA varied by 10–20, depending on the drift voltage, the experimental R_p obtained for both TEA and TBA remained almost constant and only varied by 2–4. Despite the observed differences in the experimental and theoretical R_p, resolving powers as high as 71 (~28 000 theoretical plates) were observed.

In the next set of experiments, all other experimental conditions were kept constant with the exception of the AG distance, which was reduced from 5.0 mm to 0.7 mm, with the results shown in Fig. 3. This distance was reduced in an attempt to improve the R_p of this instrument. The purpose of the anode grid is to prevent the electric field of the arriving ion cloud from inducing a capacitive current flow on the Faraday plate detector prior to ions striking the anode, thus effectively preventing the formation of an image current. These capacitive effects, determined by the distance of the anode from the anode grid, have been shown to play a significant role in the measured peak width.[31]

Similar trends to those observed with the 5.0 mm AG distance were observed in the data in Fig. 3. Each ion gate width had an optimal operational drift voltage where R_p was maximized, with larger ion gate widths (top panels) performing better at lower drift voltages and shorter ion gate widths (bottom panels) performing better at higher drift voltages. However, the difference between the theoretical and experimental R_p for the TEA ion were, on average, smaller (28, 34, 46 and 52% for ion gate widths of 800, 400, 200 and 100 µs, respectively). The maximum R_p obtained for the 0.7 mm AG distance was 94 (~49 000 theoretical plates), using a 100 µs gate width, which compared favorably with the best R_p values obtained for the 5.0 mm AG distance. It is important to note that all the data in Figs. 2 and 3 were collected with a drift gas flow rate of 0.2 L min^{-1} and a gas diffuser to minimize the contribution from laminar flow dispersion. Data collected with a drift gas flow rate of 1.5 L min^{-1} (green trace in Supplementary Figs. S1 and S2 in Supporting Information) suffered from a marked loss in resolving power caused by turbulent drift gas flow.

Resolving power measurements with a 30 mm anode were also performed (Supplementary Fig. S1 for TEA and Supplementary Fig. S2 for TBA, see Supporting Information). For this dataset, it was observed that the larger anode provided a more intense signal due to the larger ion sampling area, allowing the use of shorter ion gate widths, and that for the shorter ion gate widths, the data collected with the 10 mm anode showed a 5–10% higher resolving power due to sampling of only the most homogeneous portion of the ion packet.

DOI: 10.1002/rcm

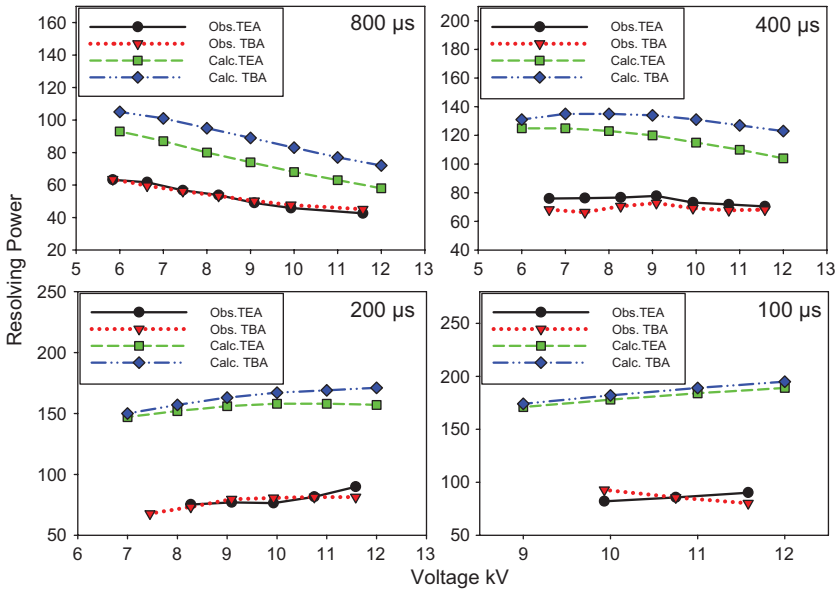

Figure 3. Theoretical and experimental resolving power (R_p) obtained for 150 µM tetrabutylammonium (TBA) nitrate and tetraethylammonium (TEA) acetate tetrahydrate solution using 800, 400, 200 and 100 µs ion gate widths and drift voltages in the range 5.84–11.58 kV for a 10 mm-diameter anode and a 0.7 mm anode grid distance instrumental configuration. The blue (diamonds) and green (squares) traces represent the theoretical R_p for TBA and TEA, respectively, while the red (triangles) and black (circles) traces represent experimentally observed values. A drift gas at a flow rate of 0.2 L min^{-1} was used.

Once the performance of the resistive-glass IMS system in terms of R_p had been investigated, the separation power in terms of chromatographic resolution was evaluated under identical conditions. Equation (1) indicates that the diffusional contribution to peak width is expected to decrease as the voltage on the drift tube is increased. At high drift voltages, the ion packet experiences less diffusional broadening and becomes progressively more similar in peak width to the initial ion packet. This is advantageous in terms of R_p, but this rapid transit through the drift region also decreases the extent of the interactions with the drift gas, negatively affecting the chemical separation power if two or more different ionic species are contained within the ion packet.

Figure 4 shows the chromatographic resolution obtained for a mixture of the TBA and TEA ions using 800, 400, 200 and 100 µs ion gate widths with drift voltages in the range 6.63–11.58 kV for a 30 mm anode, 1.5 L min^{-1} N_2 drift gas configuration. For an 800 µs ion gate width, the resolution increased with decreasing voltage, with a maximum resolution of 11.1 obtained at a drift voltage of 6.63 kV. This same trend was observed for an ion gate width of 400 µs, with a maximum resolution of 12.4 and 12.5, obtained at drift voltages of 6.63 and 7.45 kV, respectively. At shorter ion gate widths, an optimum voltage appears around 10–11 kV, producing a maximum resolution of 13.3 for a 200 µs ion gate width, and 15.2 for the 100 µs ion gate width. All the observed resolution values were baseline-resolved or better, satisfying the minimum condition $1.75 < R < 2.0$.[32,33] The chromatographic resolution values obtained using a 0.2 L min^{-1} N_2 drift gas flow rate and various anode sizes were lower on average than when 1.5 L min^{-1} flow rates were used (Fig. 4), and showed less marked trends (Supplementary Fig. S3, see Supporting Information).

Of the different configurations investigated thus far, the 30 mm anode configuration using a drift gas flow rate of 1.5 L min^{-1} N_2 produced the largest resolution, especially at shorter ion gates, and highest sensitivities. This configuration, however, produced relatively lower R_p values in

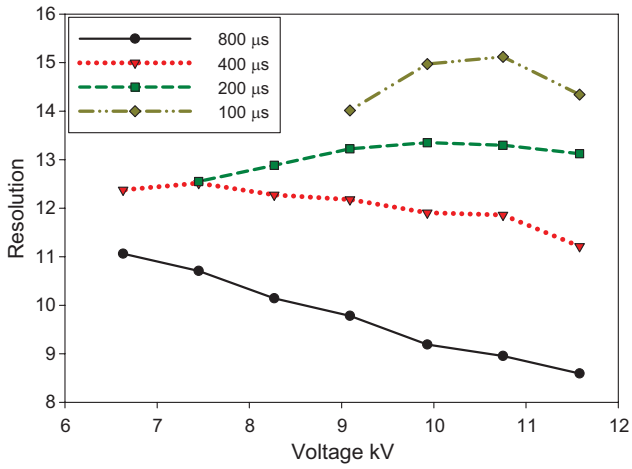

Figure 4. Chromatographic resolution obtained for an equimolar mixture of tetrabutylammonium (TBA) nitrate and tetraethylammonium (TEA) acetate tetrahydrate using 800, 400, 200 and 100 µs ion gate widths and drift voltages in the range 6.63–11.58 kV for a 30-mm-diameter anode configuration employing a drift gas flow rate of 1.5 L min^{-1} N_2.

DOI: 10.1002/rcm

RCM

almost all scenarios (Supplementary Figs. S1 and S2, see Supporting Information). In practical terms, however, it is preferable to operate under conditions that maximize resolution of pairs of chemically related species. As such, the R_p value only provides a simple assessment of the peak capacity of the system based on peak width measurements for a single ion.

To investigate the contributions to the experimental pulse width from factors such as field inhomogeneity and non-ideal gate performance in our resistive-glass IMS instrument, we applied Eqn. (2) to our voltage-dependent experimental data. First, we investigated the diffusional contribution to the final experimental pulse width observed at the detector, represented by the 'α' parameter. This parameter also models other effects that could lead to peak broadening when a fraction of the ions spend more time in the drift tube than expected. An example of this type of effect would be that caused by field inhomogeneity within the drift tube, which results in ion packet distortion. Another possibility would be interaction of the edges of the ion packet with internal components of the IMS instrument such as the ion gate mask. These types of interactions would not have a constant voltage dependence and would affect α.

Figure 5 shows plots of squared experimental peak width (w^2) as a function of the diffusion-dependent parameter (Tt_d^2/V) collected with a 30 mm anode, 1.5 L min^{-1} N_2 drift gas configuration. The color-coded lines represent the least-squares fit of the experimental data for ion gate widths of 800, 400, 200 and 100 µs. The slope of the linear equation fitting each data subset gives an estimate of α. At each gate width, the α values obtained for both TEA and TBA were very similar, as expected. However, all the experimental α values were larger than the expected 'ideal' value of 0.9×10^{-3} predicted by Eqn. (2), indicating that uncontrolled 'diffusion-like' effects made the peaks wider than expected from theory. One hypothesis to explain these results is that the electric field within the resistive-glass is less homogeneous than initially thought. Batch-to-batch performance comparisons and long-term mechanical stress and temperature stability investigations of the resistive-glass material used in this spectrometer should shed more light on this matter. In addition, changes in the resistance of the resistive-glass caused by buildup of contaminants on the surface also need to be investigated. These investigations may be complicated by the fact that electric field inhomogeneity in resistive-glass tubes would not take a periodical function form, as in stacked ring electrode spectrometers, but a much more complex three-dimensional shape. Although the α values for each respective gate width were similar, the values for different size ion gates showed a large degree of variation. The data shown in Fig. 5 also displayed an unexpected dependence of α on the initial ion gate width, with shorter ion gates having progressively larger α values of 3.9×10^{-3}, 4.3×10^{-3} and 4.9×10^{-3} V/K for gates of 400, 200 and 100 µs, respectively. We suggest that this dependence on initial ion gate width is caused by the non-ideal performance of the gating pulse shape during the opening and closing of the gate. These opening and closing events not only caused a deflection of the ion cloud away from the center of the drift space and out toward the periphery of the drift tube, but also altered the

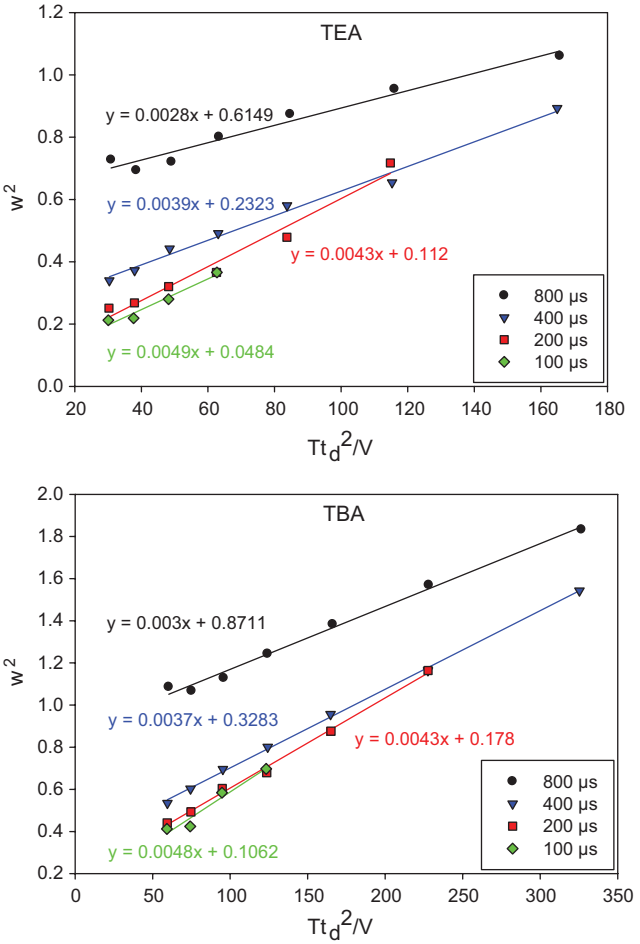

Figure 5. Measured peak width squared as a function of the diffusion-dependent parameter (α) for ion gate widths of 800, 400, 200 and 100 µs. The top panel shows results for tetra-ethylammonium (TEA) acetate tetrahydrate and the bottom panel shows results obtained for tetrabutylammonium (TBA) nitrate. The values of α are obtained from the slope of each trend line.

momentum of the ions at the leading and tailing edges of the ion packet, causing multiple 'diffusion-like' effects. Work by Puton and co-workers[23,34] showed that as the voltage on a BNG was rapidly increasing or decreasing, the electric field lines slowly shifted from perfectly parallel 'gate open' through an almost 45° angle, until the field lines joined the respective positive and negative wire sets, resulting in a 'closed gate' state. Ions traveling through these transitional field lines would be forced into a different path from that of the ion packet core. This distortion at the leading and trailing edges would add an α contribution to each individual gating event. When employing shorter ion gate pulse widths for ion injection, these leading and trailing edge distortions are relatively more significant, becoming a greater percent of the total ion gate width and resulting in a relatively more distorted ion packet. Non-ideal BNG behavior is a well-known phenomenon and has been studied experimentally[20,35,36] and via simulations.[25,37] A summary of the α values for all other experimental conditions tested is presented in Table 1 together with the corresponding 95%

DOI: 10.1002/rcm

Table 1. Values of α reported as × 10^2 (V/K) together with their corresponding 95% CI. Confidence intervals not calculated for trend lines with ≤4 data points

TEA Starting condition	800 μs gate	400 μs gate	200 μs gate	100 μs gate
30 mm anode	0.285 ± 0.024	0.328 ± 0.030	0.451 ± 0.110	0.201
30 mm anode 1.5 L min^{-1}	0.279 ± 0.058	0.395 ± 0.046	0.546 ± 0.128	0.495
10 mm anode	0.381 ± 0.027	0.418 ± 0.015	0.439 ± 0.039	0.410
10 mm anode 0.7 mm AG	0.272 ± 0.033	0.309 ± 0.020	0.476 ± 0.133	0.519
TBA **Starting condition**	**800 μs gate**	**400 μs gate**	**200 μs gate**	**100 μs gate**
30 mm anode	0.316 ± 0.031	0.345 ± 0.018	0.359 ± 0.029	0.101
30 mm anode 1.5 L min^{-1}	0.298 ± 0.029	0.373 ± 0.014	0.428 ± 0.038	0.482
10 mm anode	0.408 ± 0.035	0.427 ± 0.041	0.483 ± 0.024	0.487
10 mm anode 0.7 mm AG	0.287 ± 0.041	0.418 ± 0.059	0.553 ± 0.078	0.065

confidence intervals (CI). Although the α values were different for different experimental setups, a similar gate dependence on initial ion gate width was observed for all investigated configurations, reinforcing the idea of a gating contribution to diffusion-like peak broadening.

In order to better understand the contribution to peak width caused by any non-ideal performance of the ion gate, the experimentally observed β parameter in Eqn. (2) was also investigated. As mentioned earlier, β represents the contribution from the initial ion gate width to the final peak width measured at the detector and includes factors that would cause changes in the behavior of the ion packet depending on the amount of injected ions. For example, β values greater than 1 would point to Coulombic repulsion or other electrostatic interactions caused by increased charge density in the injected ion packet when using wider ion gate pulses. The β term would have a theoretical value of 1 only if the size of the final measured ion packet was equal in width to the initial ion packet.

Figure 6 shows plots of experimental squared peak width (w^2) as a function of the nominal squared ion gate width (t_g^2) collected with a 10 mm anode configuration. The color-coded trend lines represent the least-squares fit of the experimental data for ion gate widths of 800, 400, 200 and 100 μs, the slope for each individual gate being an estimation of β in each case. All the observed β values were lower than unity, but behaved more ideally for TBA than for TEA. The smaller than expected values of β obtained with our resistive-glass IMS instrument indicate that the peak width measured at the detector is narrower then the width of the initially injected ion packet. Previous work by Siems *et al.*[19] and Spangler and Collins[31] showed an opposite effect, with β values of 1.13–1.24 and 1.15, respectively. In addition to these general trends, the β values for both TBA and TEA showed an unexpected dependence on the drift voltage. The largest value of $\beta = 0.547$ for TEA was observed at a drift voltage of 11.6 kV with progressively smaller values occurring at lower voltages. For TBA, the largest value of $\beta = 0.929$ was obtained at a drift voltage of 11.6 kV, with the smallest value of $\beta = 0.729$ obtained at a drift voltage of 8.3 kV.

In our setup, the ion gate is closed by applying ±35 V to the adjacent ion gate wire sets floating at the drift tube entrance voltage. During the time period when the ion gate is closed, depletion of the incoming ion cloud in the area immediately behind the gate occurs. When employing shorter ion gate pulse widths, this ion-depleted area in space becomes relatively more significant because the proportion of depleted

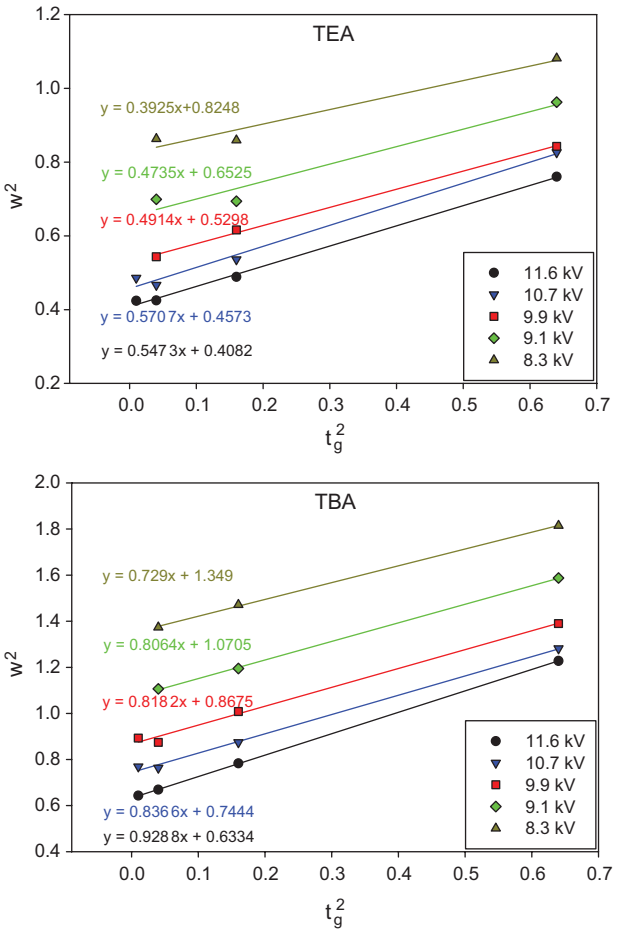

Figure 6. Measured squared peak widths as a function of the ion gate width at drift voltages of 11.6, 10.7, 9.9, 9.1 and 8.3 kV. The top panel shows results obtained for tetraethylammonium (TEA) acetate tetrahydrate and the bottom panel shows results obtained for tetrabutylammonium (TBA) nitrate. The values of β are obtained from the slope of each trend line.

DOI: 10.1002/rcm

RCM

ions becomes a greater percentage of the total amount of ions to be injected, reducing the value of β. Because the voltage drop in the desolvation chamber preceding the ion gate increases when the drift voltage is increased, it is expected that the depletion region will be replenished faster at higher drift voltage settings, explaining the trend towards higher β values. We also hypothesize that the observed differences between ions with different m/z values is related to the voltage used to close the ion gate. It appears as if the ± 35 V applied to the BNG is insufficient to deflect all the ionic species in the incoming ion beam correctly. This would explain why the β value from the smaller, faster-moving TEA species is approximately half of the β value associated with the larger and slower moving TBA ion, which behaves almost ideally at higher drift voltages. Limitations in the ion gate pulsing electronics prevented us from applying higher gating voltages to further test this hypothesis.

CONCLUSIONS

Our studies have shown that the optimum resolving power in the prototype resistive-glass ion mobility instrument discussed here is dependent on voltage and initial ion gate pulse width, with values that are lower than predicted by theory by 25–48%, with larger deviations occurring at shorter ion gate widths. The performance of the resistive-glass spectrometer was found to be comparable with that of other standalone stacked ring spectrometers reported in the literature, which typically produce resolving powers approximately 26–46% lower than that predicted by theory.[38] The anode grid to anode distance has a major effect on the resolving power, as decreasing this distance from 5.0 to 0.7 mm produced an average increase in resolving power of 20, with larger gains at shorter ion gate pulse widths, due to the decoupling of the image current from ion detection.

The separation power in terms of chromatographic resolution showed that a high drift gas flow rate was the most important factor benefiting separation. Our results also showed that at large initial ion gate pulse widths, better separations could be obtained at lower drift voltages. However, as the size of the ion gate pulse decreased to values of ≤ 200 μs, a voltage-dependent optimum appears at a drift voltage between 10 and 11 kV.

Through an analysis of both the initial ion gate pulse width dependence of the α value, and the smaller than expected β values obtained with our instrument, we have uncovered imperfections in the behavior of our current ion gating system which will be addressed in future instrument versions.

SUPPORTING INFORMATION

Additional supporting information may be found in the online version of this article.

REFERENCES

1. Cohen MJ, Karasek FW. *J. Chromatogr. Sci.* 1970; **8**: 330.
2. Eiceman GA, Karpas Z. *Ion Mobility Spectrometry*, (2nd edn). CRC Press: Boca Raton, 2005.
3. Hagen DF. *Anal. Chem.* 1979; **51**: 870.
4. Clowers BH, Dwivedi P, Steiner WE, Hill HH, Bendiak B. *J. Am. Soc. Mass Spectrom.* 2005; **16**: 660.
5. Ruotolo B, Verbeck GF, Thomson LM, Gillig KJ, Russell DH. *J. Am. Chem. Soc.* 2002; **124**: 4214.
6. Wyttenbach T, Paizs B, Barran P, Breci L, Liu D, Suhai S, Wysocki VH, Bowers MT. *J. Am. Chem. Soc.* 2003; **125**: 13768.
7. Badman ER, Hoaglund-Hyzer CS, Clemmer DE. *Anal. Chem.* 2001; **73**: 6000.
8. Barran PE, Polfer NC, Campopiano DJ, Clarke DJ, Langridge-Smith PRR, Langley RJ, Govan JRW, Maxwell A, Dorin JR, Millar RP, Bowers MT. *Int. J. Mass Spectrom.* 2005; **240**: 273.
9. Steiner WE, Harden CS, Hong F, Klopsch SJ, Hill HH, McHugh VM. *J. Am. Soc. Mass Spectrom.* 2006; **17**: 241.
10. Ewing RG, Atkinson DA, Eiceman GA, Ewing GJ. *Talanta* 2001; **54**: 515.
11. Budimir N, Weston DJ, Creaser CS. *Analyst* 2007; **132**: 34.
12. Wu C, Siems WF, Hill HH. *Anal. Chem.* 2000; **72**: 396.
13. Miki A, Keller T, Regenscheit P, Dirnhofer R, Tatsuno M, Katagi M, Nishikawa M, Tsuchihashi H. *J. Chromatogr. B* 1997; **692**: 319.
14. Keller T, Keller A, Tutsch-Bauer E, Monticelli F. *Forensic Sci. Int.* 2006; **161**: 130.
15. Kanu AB, Hill HH, Gribb MM, Walters RN. *J. Environ. Monit.* 2007; **9**: 51.
16. Liu XY, Valentine SJ, Plasencia MD, Trimpin S, Naylor S, Clemmer DE. *J. Am. Soc. Mass Spectrom.* 2007; **18**: 1249.
17. Valentine SJ, Plasencia MD, Liu XY, Krishnan M, Naylor S, Udseth HR, Smith RD, Clemmer DE. *J. Proteome Res.* 2006; **5**: 2977.
18. McLean JA, Ruotolo BT, Gillig KJ, Russell DH. *Int. J. Mass Spectrom.* 2005; **240**: 301.
19. Siems WF, Wu C, Tarver EE, Hill HH, Larsen PR, McMinn DG. *Anal. Chem.* 1994; **66**: 4195.
20. Kwasnik M, Fuhrer K, Gonin M, Barbeau K, Fernandez FM. *Anal. Chem.* 2007; **79**: 7782.
21. Laprade BN. In *The 2004 Pittsburgh Conference on Analytical Chemistry and Applied Spectroscopy*. Chicago, IL, 2004.
22. Photonis. *A Direct Comparison of a Resistive Glass and Stacked Ring Reflectron*. Available: http://www.photonis.com/data/cms-resources/File/new/Glass%20Reflectron%20-%20 ASMS%202006.pdf.
23. Puton J, Knap A, Siodlowski B. *Sens. Actuators B* 2008; **135**: 116.
24. Dahl DA, McJunkin TR, Scott JR. *Int. J. Mass Spectrom.* 2007; **266**: 156.
25. Lai H, McJunkin TR, Miller CJ, Scott JR, Almirall JR. *Int. J. Mass Spectrom.* 2008; **276**: 1.
26. Bradbury NE, Nielsen RA. *Phys. Rev.* 1936; **49**: 388.
27. Revercomb HE, Mason EA. *Anal. Chem.* 1975; **47**: 970.
28. Carrico JP, Sickenberger DW, Spangler GE, Vora KN. *J. Phys. [E]* 1983; **16**: 1058.
29. Spangler GE, Vora KN, Carrico JP. *J. Phys. [E]* 1986; **19**: 191.
30. Watts P, Wilders A. *Int. J. Mass Spectrom. Ion Processes* 1992; **112**: 179.
31. Spangler GE. *Int. J. Mass Spectrom.* 2002; **220**: 399.
32. Matz LM, Hill HH. *Anal. Chem.* 2002; **74**: 420.
33. Hall G, Dolan JW. *LCGC North Am.* 2002; **20**: 842.
34. Tadjimukhamedov FK, Puton J, Stone JA, Eiceman GA. *Rev. Sci. Instrum.* 2009; **80**: 103103:1.
35. Kimmel JR, Fernandez FM, Zare RN. *J. Am. Soc. Mass Spectrom.* 2003; **14**: 278.
36. Clowers BH, Siems WF, Hill HH, Massick SM. *Anal. Chem.* 2006; **78**: 44.
37. Xu J, Whitten WB. *Int. J. Ion Mobil. Spectrom.* 2008; **11**: 13.
38. Kanu AB, Gribb MM, Hill HH. *Anal. Chem.* 2008; **80**: 6610.

DOI: 10.1002/rcm